JOURNAL OF MATERIALS SCIENCE 35 (2000) 6111–6121

Influence of molecular weight on the mechanical performance of a thermoplastic glassy polyimide

L. M. NICHOLSON
Institute for Computer Applications in Science and Engineering, NASA Langley Research Center, MS 132C, 3 West Reid Street, Hampton, VA 23681-2199, USA
E-mail: l.m.nicholson@larc.nasa.gov

K. S. WHITLEY, T. S. GATES*
Mechanics and Durability Branch, Structures & Materials Competency, NASA Langley Research Center, MS 188E, 2 West Reid Street, Hampton, VA 23681-2199, USA
E-mail: t.s.gates@larc.nasa.gov

J. A. HINKLEY
Applied Materials and Processes Branch, Structures & Materials Competency, NASA Langley Research Center, MS 188E, 2 West Reid Street, Hampton, VA 23681-2199, USA

Mechanical testing of an advanced thermoplastic polyimide (LaRC^{TM}-SI) with known variations in molecular weight was performed over a range of temperatures below the glass transition temperature. The physical characterization, elastic properties and notched tensile strength were all determined as a function of molecular weight and test temperature. It was shown that notched tensile strength is a strong function of both temperature and molecular weight, whereas stiffness is only a strong function of temperature. A critical molecular weight (M_c) was observed to occur at a weight-average molecular weight ($\bar{M}_w$) of ~22000 g/mol below which, the notched tensile strength decreases rapidly. This critical molecular weight transition is temperature-independent. Furthermore, inelastic analysis showed that low molecular weight materials tended to fail in a brittle manner, whereas high molecular weight materials exhibited ductile failure. The microstructural images supported these findings.

1. Introduction

The replacement of metals and glass in high performance applications with polyimides has been an escalating trend since their inception due to their outstanding mechanical and thermal properties [1]. Aromatic polyimides are thermally stable high performance polymers that are used in a variety of forms, most of which are commercially available: composite matrices, adhesives, coatings, films and fibers.

Engineers strive for optimal mechanical properties with a minimum of weight in the design and production of advanced structural materials. Recent demands of the aerospace industries for high temperature and high-performance polymers, have led to the development of structurally modified polyimides suitable as composite matrix resins used in load-bearing applications. These novel polymer matrix composites (PMCs) are amorphous in texture and with the abundance of aromatic rings in the polymer, the increased chain stiffness produces a high glass transition temperature (T_g). The use of PMCs in airframe structure can give up to 40% weight savings along with a reduction in the number of parts [2].

There has been a wealth of polyimides in aerospace applications, but there are still some reservations about their extensive exploitation in structural composites, in part due to their inherent high cost. Maintaining strength and/or stiffness while improving processability is a familiar issue for polymer design engineers. Both processing and performance are intrinsically linked to the polymer's molecular weight. While decreasing the molecular weight will enhance a material's processability, the resulting product can have low fracture toughness and inferior damage resistance, assumed to be due to the brittle nature of the polymer below its glass transition temperature (T_g) [3]. Matsuoka [4] noted that in the glassy state, the molecular weight affects the toughness and impact strength of the polymer; impact strength increases with increase in molecular weight. Previous studies on "Kapton^{TM}-like" (DuPont) polyimide films [5–7] have shown that the mechanical properties were both process and material specific. Currently, there is

* Author to whom all correspondence should be addressed.

no unified understanding of exactly how the intrinsic chemical and physical properties of the polymer affect the resultant mechanical performance. The ability to predict performance using intrinsic properties as inputs would greatly enhance the efficiency of design and development of PMCs. Data from experiments can serve as a basis for model construction and provide material properties required by the selected model. One of the first steps in the construction of a model is the careful experimental correlation of thermo-mechanical behavior of a well-characterized polymer to known changes in intrinsic properties.

The objective of this paper is to detail and summarize the physical and mechanical testing of an advanced polymer (LaRC^{TM}-SI). Using five known variations in molecular weight, the results of mechanical tests were compared over a range of temperatures below the glass transition. Results from these tests will be presented along with descriptions of the material, test methods and an interpretation of the polymer's mechanical response.

2. Experimental details

2.1. Materials

The materials used in this study were prepared by Imitec Inc., Schenectady, NY, and received in powder form. LaRC^{TM}-SI (NASA Langley Research Center-Soluble Imide) was synthesized from 4,4′-oxydiphthalic anhydride (ODPA), 3,3′,4,4′-biphenyltetracarboxylic dianhydride (BPDA) and 3,4′-oxydianiline (3,4′-ODA). Stoichiometric imbalances, designated by percentage offsets [8], were controlled by reacting an excess of the diamine with an appropriately reduced quantity of the dianhydrides in *N*-methyl-2-pyrrolidinone (NMP). The oligomers were endcapped with phthalic anhydride (PA). The synthesis route is illustrated in Fig. 1, and more extensive synthesis descriptions of this material have been published elsewhere [9, 10]. Molecular weights were determined on the as-received imide powders using gel permeation chromatography and differential viscometry (GPC/DV) [8]. A summary of the results obtained from GPC/DV measurements on the LaRC^{TM}-SI samples is shown in Table I; the notable inclusions are the weight-average molecular weight ($\overline{M}_w$) and the polydispersity index.

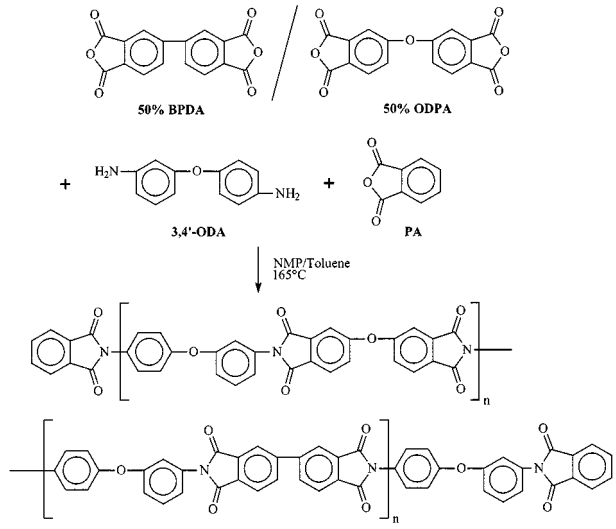

Figure 1 Synthetic scheme of LaRC^{TM}-SI.

2.2. Characterization

The powder was dried under vacuum at 215°C for 48 hours to remove any residual solvents prior to being compression molded in air. Thermogravimetric analysis (TGA) was conducted on a Seiko TG/DTA 220 in isothermal and dynamic modes in air, at a heating rate of 2.5°C/min up to 650°C. The results showed that the as-received powder was more than 99% free of excess solvent and after drying, more than 99.5% free. The dried powder was placed in a 152 × 152 mm stainless steel mold lined with Kapton^{TM} (DuPont) film, spray-coated with Frekote^{TM}33-NC release agent. Neat resin panels were formed isothermally at 340°C for one hour under 3.1 MPa of pressure. Mechanical test coupons measuring approximately 150 × 17.5 × 5.8 mm were machined from the panels. Differential scanning calorimetry (DSC) was performed using a Perkin Elmer DSC 7 to determine the glass transition temperature (T_g) of the molded material. Polymer sample weights of 2–5 mg were used under a nitrogenous atmosphere at a heating rate of 10°C/min. The glass transition temperature was taken at the inflection point in the heat flow versus temperature curve and an average of three samples used to determine the T_g for each molecular weight variation. These results are contained in Table II, along with glass transition temperatures measured using dynamic mechanical analysis (DMA) and DSC, reproduced from Siochi [8]. Also contained in this table are coefficients of linear thermal expansion (CTE) as measured by laser dilatometry.

2.3. Mechanical test instrumentation and procedures

The goal of the mechanical tests was to determine the elastic properties and notched tensile strength as

TABLE I Molecular weights and intrinsic viscosities for cured LaRC^{TM}-SI resin specimens. The stoichiometric offset is incrementally increased to effect a decrease in Molecular weight. Reproduced from Siochi [8]

% Offset	$\overline{M}_w$ (g/mol)	$\overline{M}_n$ (g/mol)	$\frac{\overline{M}_w}{\overline{M}_n}$	$\overline{M}_z$ (g/mol)	$\overline{M}_v$(g/mol)	Intrinsic Viscosity (m^3/kg)
0	58900	11450	5.14	107350	43035	0.58×10^{-4}
1	51070	11180	4.57	87130	37530	0.60×10^{-4}
2	41100	13770	2.98	75703	31675	0.47×10^{-4}
3	24290	10560	2.30	43955	19170	0.36×10^{-4}
4	21180	10405	2.04	39110	17155	0.33×10^{-4}
5	15880	8882	1.79	26935	13690	0.27×10^{-4}

TABLE II Glass transition (T_g) temperatures measured on the cured LaRC™-SI resin specimens by differential scanning calorimetry (DSC) and dynamic mechanical analysis (DMA); after [8]. Coefficients of linear thermal expansion (CTE) calculated by Laser dilatometry are also presented. Static mechanical test temperatures (°C) are calculated as an interval from below the T_g. ($\Delta T = T_g$–Test Temperature); * indicates that the actual test temperatures deviated from ΔT by no more than a few Kelvin

Offset %	$\overline{M}_w$ (g/mol)	T_g (DSC) °C	T_g (DMA) °C	Avg CTE $\mu\varepsilon$/K	St.dev. CTE $\mu\varepsilon$/K	$\Delta T =$ 15 K	$\Delta T =$ 25 K	$\Delta T =$ 45 K	$\Delta T =$ 70 K	$\Delta T =$ 120 K
0	58900	239	253	45.93	0.17	—	—	—	—	—
1	51070	248	258	45.72	0.12	235	225	205	180	130
2	41100	248	250	47.04	0.77	231	221	201	176	126
3	24290	242	249	46.04	1.44	223	213	193	168	118
4	21180	230	246	46.18	1.57	223	213	193	177*	126*
5	15880	231	—	46.27	0.11	219	209	189	164	114

a function of molecular weight and test temperature. Uniaxial tensile tests were performed at six specific test temperatures below the glass transition temperature (T_g). For comparison purposes, the test temperature is referenced to the glass transition temperature, as defined below:

$$\Delta T = T_g - T_{test} \tag{1}$$

A high-temperature strain gage was applied to each specimen in a direction transverse to the length, on the face of the specimen. The specimen and gage were subsequently dried at 110°C for 120 hours and the gage-bonding agent post-cured at 210°C for 2 hours. Longitudinal strain was measured using a high-temperature, knife-edge extensometer mounted at the specimen's center, on the thin edge of the specimen. The output voltages from the strain gages were filtered and amplified by a strain gage conditioner before the conditioned output was collected by the digital data acquisition system.

The tensile tests were performed using a 22.2 kN servo-hydraulic test system equipped with a heated test chamber. The specimens were enclosed in the chamber and mounted in mechanical wedge type grips. During the course of a test, temperature was monitored with several thermocouples placed near the specimen. The temperature was allowed to equilibrate before a tensile load was applied at a constant ramp rate of 22.2 N/s. The tests were terminated when failure occurred or the maximum elongation was achieved.

The engineering stress on the specimen was determined from the load measured by the servo-hydraulic system's load cell, divided by the average cross-sectional area measured prior to the test. Each recorded elastic modulus measurement is an average of at least three replicates of each molecular weight at each test temperature.

2.3.1. Notched tensile strength

For a given molecular weight, two tests at each temperature were performed using the notched specimen geometry. To facilitate a controlled failure, an edge notch was cut in the specimen using a jeweler's blade (0.38 mm width) mounted on a handsaw. The notch was placed on one side only, at 44 mm from the bottom grip and extended approximately 2 mm in from the free edge. Tensile strength was calculated from the maximum load achieved during the tensile test divided by the original, unnotched cross sectional area. Photomicrographs with a magnification of 25×, were taken of the notched surface after failure to determine the morphology of the failure surface.

2.3.2. Elastic properties

Young's Modulus, (E) was calculated using Equation 2 from the least squares fit to the slope of the linear portion of the stress, (σ), versus the longitudinal strain, (ε_x), curve, fitting through the origin. Similarly, Poisson's Ratio (ν), Equation 3, was calculated as the slope of the transverse strain (ε_y), versus the longitudinal strain in the same linear region. The Shear Modulus (G) was calculated in terms of E and ν using Equation 4.

$$E = \frac{\sigma_x}{\varepsilon_x} \tag{2}$$

$$\nu = -\frac{\varepsilon_y}{\varepsilon_x} \tag{3}$$

$$G = \frac{E}{2(1+\nu)} \tag{4}$$

2.3.3. Inelastic behavior and determination of yield point

For all test specimens, the complete stress-strain data during loading were recorded. In many cases, the notched specimens exceeded 2% strain to failure. For a given molecular weight, one unnotched specimen was tested at each temperature to inelastic strain levels of at least 2% strain. The combined data sets from the notched and unnotched tests were used to characterize the inelastic behavior of the resin.

At the macroscopic level, it is assumed that the material is isotropic [11, 12]. This assumption is based on the fact that although there may be some low-level anisotropy at sub-molecular scales, this does not greatly influence macroscopic bulk properties at relatively low strains and at temperatures below the glass transition. Therefore, if it is assumed that the resin is an isotropic material, the total strain in the specimen can be resolved into an elastic and plastic incremental strain component:

$$d\varepsilon = d\varepsilon^e + d\varepsilon^p \tag{5}$$

where ε^e is the elastic strain and ε^p is the plastic strain. For an isotropic, strain hardening type of material such as LaRC™-SI, it was assumed that the plastic strain

is a function of the applied stress and can be evaluated from the difference in the total strain and the elastic strain:

$$\varepsilon^{\mathrm{p}} = \varepsilon - \varepsilon^{\mathrm{e}} = f(\sigma) \tag{6}$$

The elastic strain component is derived from the rearrangement of the expression for the Young's Modulus. The plastic strain component can be modeled using a power law expression with two empirical constants (A and n) such that:

$$\varepsilon^{\mathrm{p}} = A\sigma_x^n \tag{7}$$

For the uniaxial loading case, the total strain relationship is now given as

$$\varepsilon = \frac{\sigma_x}{E} + A\sigma_x^n \tag{8}$$

Thus, Equation 8 is a composite function that contains relations to account for the elastic and plastic portions of the stress-strain curve. The plastic strain constants (A and n) were evaluated using a least squares fit of the stress-strain curves for each test temperature through Equation 8. Having obtained values for A and n for each test temperature, the average exponent, n, was calculated for the entire data set. This value for n was then used to re-fit the stress-strain curves with Equation 8 and consequently a new constant (A) was found for each temperature. These values are tabulated in Table III.

The LaRC$^{\mathrm{TM}}$-SI material is, in general, a nonlinear material that may exhibit plastic behavior at relatively low strain levels. It was observed, however, that even at elevated temperatures the elastic portion dominated at small strains, whereas at larger strain levels the plastic portion became dominant. For the consideration of failure mechanisms in the material, it is necessary to establish a material yield point. This yield point can then be compared to the failure point and transitions between brittle and ductile behavior become more apparent.

The distinction between elastic or viscoelastic (recoverable) and plastic (permanent) deformation is not easily resolved experimentally. The practical determination of the yield point on a polymer stress-strain curve, is where the maximum occurs and is referred to as the *intrinsic yield point* [13]. This definition cannot be applied to strain-hardening polymers that have a stress-strain curve without a maximum. The conventional concept of a yield point is defined as the point at which the deformation ceases to be entirely elastic. On the stress-strain curve, this occurs where the curve deviates from linearity. This point is more generally known as the *limit of proportionality*, and is where the material exhibits incipient inelastic behavior.

It was felt, therefore, that the simple expression in Equation 8 was sufficient to describe the strain-hardening type of behavior observed over the range of test temperatures. Equation 8 assumes that the yield point is equivalent to the limit of proportionality; the

TABLE III Mechanical properties for LaRC$^{\mathrm{TM}}$-SI. Mechanical test temperatures (T_t) and the indicated property: averaged Young's Modulus (E) as given in Equation 2; averaged Poisson's ratio (ν) as expressed in Equation 3; averaged Shear Modulus (G) calculated using Equation 4; and averaged notched tensile strength (NTS). Plastic strain components: constants (A) calculated for exponent ($n = 2.75$) as used in Equation 7. Yield stress (σ_o) as given in condition (10)

$\overline{M}_w$ (g/mol)	T_t [°C]	ΔT [K]	Av. E [GPa]	Av. ν	Av. G [GPa]	Av. NTS [MPa]	A [(MPa)$^{-n}$]	σ_o [MPa]
51070	23	227	3.764	0.384	1.360	63.850	2.47E-08	36.34
	130	120	2.755	0.391	0.990	63.526	6.28E-08	25.48
	180	70	2.480	0.381	0.898	49.644	7.47E-08	24.50
	205	45	2.502	0.383	0.904	39.558	2.79E-07	11.48
	225	25	2.150	0.355	0.793	30.032	7.14E-07	7.32
	235	15	1.777	0.359	0.654	22.926	2.06E-06	4.45
41100	23	223	3.893	0.424	1.361	69.861	3.15E-08	31.02
	126	120	2.778	0.383	1.004	64.458	5.03E-08	28.79
	176	70	2.685	0.402	0.958	53.355	7.85E-08	22.76
	201	45	2.457	0.379	0.891	41.433	1.31E-07	17.87
	221	25	2.293	0.376	0.833	32.453	3.86E-07	10.03
	231	15	1.830	0.350	0.678	24.626	1.86E-06	4.64
24290	23	215	3.828	0.400	1.367	66.697	2.91E-08	32.77
	118	120	3.060	0.411	1.084	50.224	6.98E-08	22.59
	168	70	2.587	0.353	0.956	34.425	5.72E-08	27.86
	193	45	2.535	0.378	0.920	29.651	1.05E-07	19.92
	213	25	2.303	0.369	0.841	21.388	3.32E-07	10.90
	223	15	2.191	0.389	0.789	29.588	7.87E-07	6.85
21180	23	215	3.836	0.414	1.356	47.538	1.52E-08	47.44
	126	120	3.049	0.395	1.093	27.985	3.79E-08	32.09
	177	70	2.837	0.369	1.036	10.812	2.93E-08	27.50
	193	45	2.550	0.407	0.906	9.606	1.15E-07	18.85
	213	25	2.369	0.416	0.836	13.852	2.58E-07	12.39
	223	15	1.898	0.368	0.694	7.537	1.60E-06	4.96
15880	23	211	3.773	0.380	1.367	33.502	1.70E-08	44.92
	114	120	3.188	0.399	1.139	12.416	9.34E-08	18.69
	164	70	2.878	0.394	1.032	6.829	3.78E-07	8.91
	189	45	2.501	0.353	0.924	4.620	7.45E-07	6.55
	209	25	2.434	0.377	0.884	4.760	1.10E-06	5.33
	219	15	2.056	0.351	0.761	2.983	1.63E-06	4.69

departure from recoverable deformation. The constant (A) and the average exponent ($n = 2.75$) (Table III) were used to determine the yield stress for each test case. For experimental stress-strain data that is not designated to be used in design of critical components, the choice of the material yield criteria is somewhat arbitrary and may be chosen to illustrate an observed characteristic such as ductile-to-brittle transitions. Data from the stress-strain behavior of all test specimens, such as those shown in Figs 2 and 3, lead to the establishment of the following yield criteria:

$$\text{assume yield when } \left(\frac{\varepsilon^{\mathrm{p}}}{\varepsilon^{\mathrm{e}}}\right) \geq 0.05 \qquad (9)$$

Therefore, the yield stress (σ_o) can be found by solving numerically for the applied stress such that:

$$\sigma = \sigma_o \quad \text{when} \left[\frac{A\sigma_x^n}{(\sigma_x/E)}\right] = 0.05 \qquad (10)$$

The values of the Young's Modulus and the plastic strain constants, as given by Equation 8, are contained in Table III, along with the calculated yield stress and notched tensile strength for each test temperature.

3. Results

3.1. Elastic properties

The experimental results are presented for the mechanical behavior on the LaRC$^{\mathrm{TM}}$-SI specimens. The effects of variations in test temperature and molecular weight were examined for each property of interest. The error bars indicate the standard deviation of averaged results. The differences between samples of varying molecular weight were more easily discerned when weight averages are used.

Typical stress-strain curves obtained from unnotched specimens with various molecular weights, tested at the highest test-temperature of 15 K below T_{g} ($\Delta T = 15$ K) are displayed in Fig. 2a. Curves were truncated at 2.5% strain and those curves that terminate before this value, indicate failure occurred in the sample. It can be seen that the failure strains are over 0.5% for low molecular weights and the higher molecular weights have strains of at least 2.5%. Fig. 2b is a similar plot containing information for the notched specimens. There is little difference in the overall stress-strain response between the two graphs – a high degree of curvature indicates nonlinearity at the higher strains. Fig. 3a and b are analogously similar to Fig. 2, (unnotched and notched, respectively) but are conducted at room temperature ($\Delta T = 235$ K). The overall stress-strain response is effectively linear over the same strain interval (c.f. Fig. 2). The unnotched specimens (Fig. 3a) showed very slight curvature over the strain range (of up to 2.5%), whereas the notched specimens (Fig. 3b) failed at lower strains. In contrast to Fig. 2, the data in Fig. 3a and b show good uniformity with little molecular weight-dependent separation of the curves. The stress-strain responses for high and low molecular weights ($\overline{M}_{\mathrm{w}} = 51070$ g/mol, $\overline{M}_{\mathrm{w}} = 15880$ g/mol,) were plotted to display the effect of temperature. The results are shown in Fig. 4a and b,

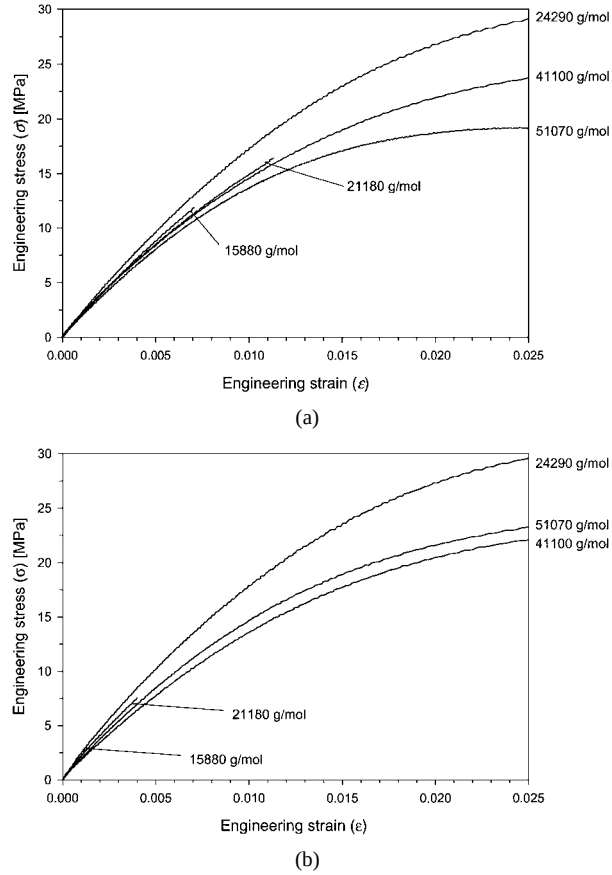

Figure 2 Stress-strain curves for (a) unnotched and (b) notched specimens of different molecular weights at a test temperature of 15 K below T_{g}. Each curve represents a single test specimen per molecular weight. Curves that terminate before the 2.5% strain level indicate failure.

respectively. Both graphs show an increase in compliance with increasing temperature. The higher molecular weight material of Fig. 4a exhibits greater elongation to failure compared to the lower molecular weight material in Fig. 4b, which tends to fail at very low strains of around 0.5%.

Young's Modulus (E) and Shear Modulus (G) versus temperature are given in Fig. 5. As expected, both E and G decrease as temperature is raised. The rate of change of E with temperature is fairly uniform up to 200°C. From 200°C to the highest temperature (∼235°C) there was a sharp decrease in modulus because the temperature was in the vicinity of the material's T_{g}. Similar to E, there is a uniform decrease in G as the temperature is raised, but with a shallower gradient. The start of the sharp decrease in modulus occurs at a higher temperature of ∼220°C. Common to both data sets is the fact that the low molecular weight materials lose their mechanical properties at a slower rate initially than the high molecular weight material. This can be seen more clearly in the Young's Moduli of Fig. 5, by the separation of the high and low molecular weight curves in the temperature range from 20–120°C. Although this trend in the material behavior is apparent, the scatter in the error bars is quite large for this temperature range, and would suggest that the curve separation is not an intrinsic property of the material.

The variations of E and G with molecular weight are shown in Figs 6 and 7. A linear least squares fit

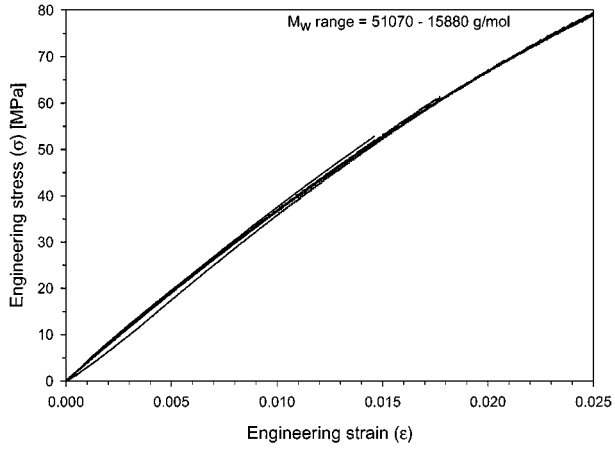

(a)

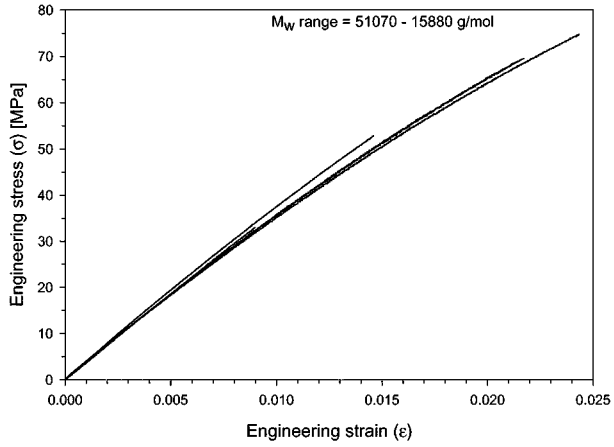

(b)

Figure 3 Stress-strain curves for (a) unnotched and (b) notched specimens of different molecular weights tested at room temperature (∼235 K below T_g). Each curve represents a single test specimen per molecular weight. Curves that terminate before the 2.5% strain level indicate failure.

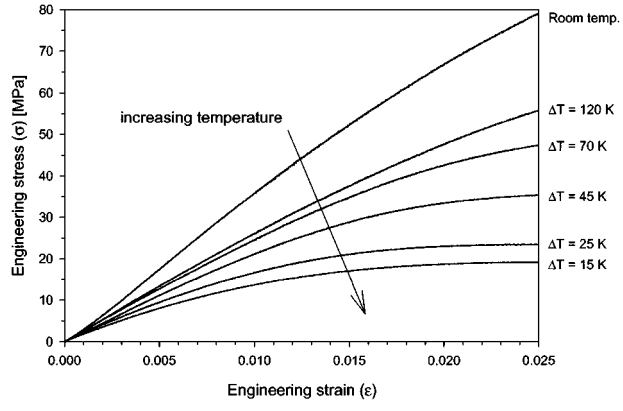

(a)

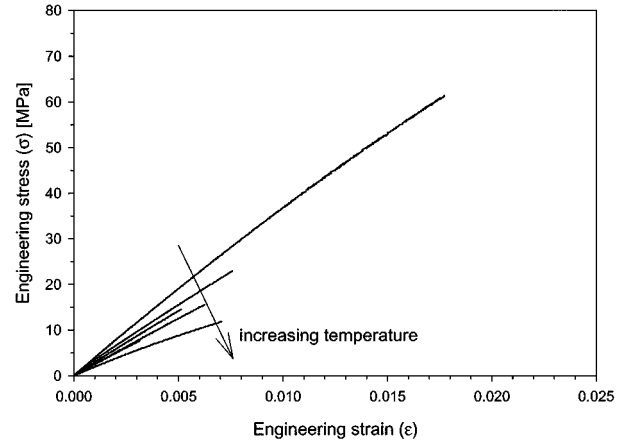

(4)

Figure 4 Stress-strain curves for unnotched specimens of (a) high molecular weight ($\overline{M}_w = 51070$ g/mol) and (b) low molecular weight ($\overline{M}_w = 15880$ g/mol) displaying the effects of different test temperatures below T_g. Each curve represents a single test specimen per molecular weight. Curves that terminate before the 2.5% strain level indicate failure. The temperature intervals for (b) are the same as those indicated in (a).

has been applied to each temperature data set. It can be seen that there is a slight decrease in the Young's Modulus and Shear Modulus as molecular weight increases, for data sets at temperatures other than room temperature. In addition, both figures illustrate the temperature dependence of each modulus; modulus decreases as temperature increases.

Graphs of notched tensile strength (NTS) versus temperature and molecular weight are shown in Figs 8 and 9, respectively. Fig. 8 illustrates the marked dependence of NTS on temperature. Thus, it is shown that NTS decreases as temperature increases. Over the range from room temperature to 150°C, the two highest molecular weight materials show good strength stability compared to the lower molecular weight materials, which show a steep decrease in strength with increase in temperature. However, in the range from 150°C to 230°C the converse is true, with the lower molecular weight materials showing little or no temperature-dependency on NTS. The NTS of the high molecular weight materials is seen to decline rapidly in this high temperature region. The different molecular weight series are fitted with least squares quadratic polynomials to indicate the nonlinear mechanical response as temperature is raised. Interestingly, the curves of the high molecular weight materials show a convex curvature, whereas the curves

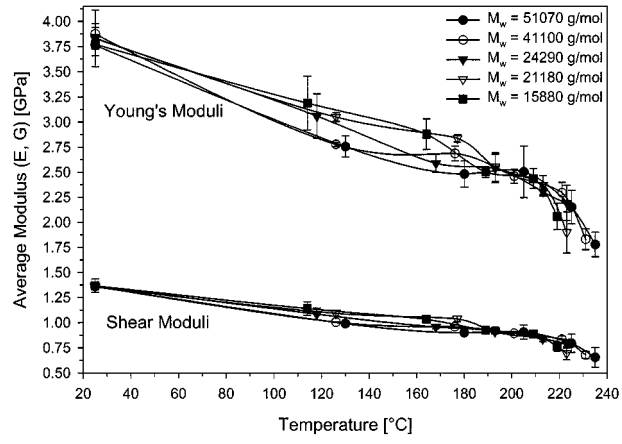

Figure 5 Averaged Young's and Shear Moduli plotted as a function of temperature for various molecular weights. Three test specimens were used to calculate the average Young's and Shear Moduli.

of the lower molecular weight materials show a concave curvature.

The NTS data plotted as a function of molecular weight, as shown in Fig. 9, have been fitted with least squares sigmoidal curves for each temperature series. It can be seen that there is a sharp increase in NTS occurring at ∼22000 g/mol weight-average molecular weight. At molecular weights higher than this

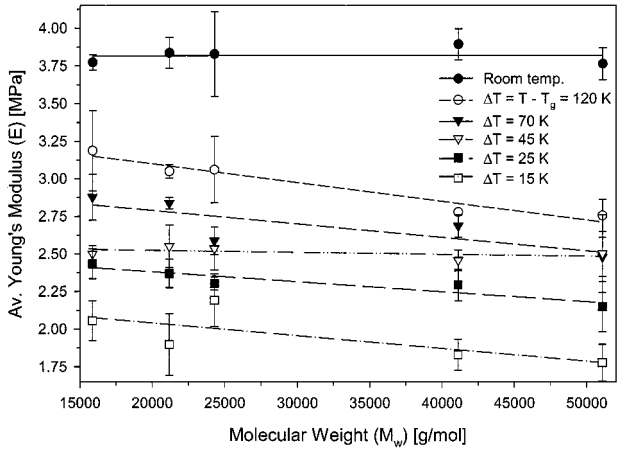

Figure 6 Averaged Young's Moduli plotted as a function of molecular weight at various temperature intervals. Three test specimens were used to calculate the average Young's Modulus.

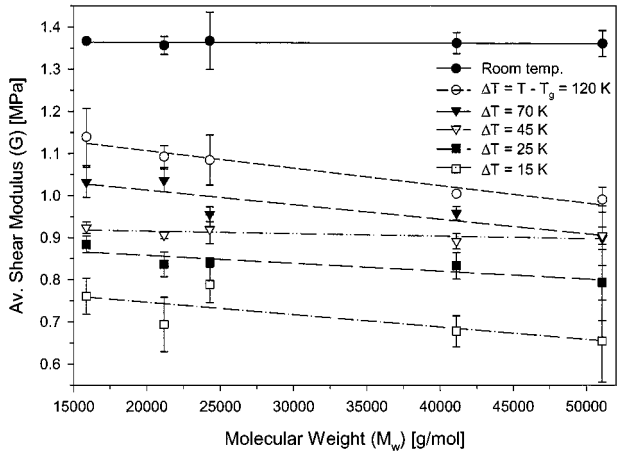

Figure 7 Averaged Shear Moduli plotted as a function of molecular weight at various temperature intervals. Three test specimens were used to calculate the average Shear Modulus.

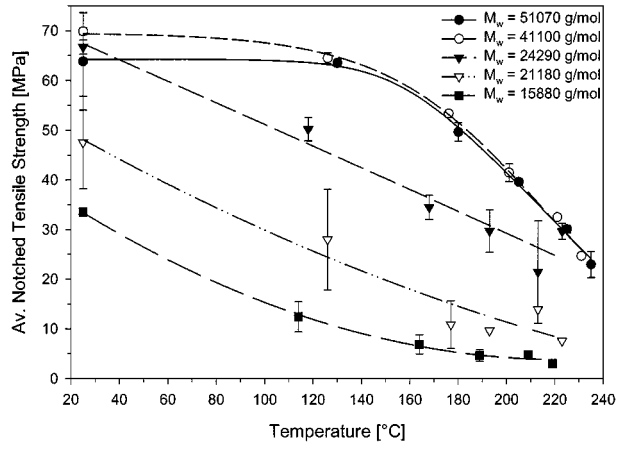

Figure 8 Averaged notched tensile strength plotted as a function of temperature for various molecular weights. Two test specimens were used to calculate the average notched tensile strength.

"critical molecular weight" (M_c) transition, the NTS is increased and conversely, at lower molecular weights ($\overline{M}_w < 22000$ g/mol), the NTS is reduced. Furthermore, this critical molecular weight transition is not temperature-dependent. The percentage change in NTS, in going from $\overline{M}_w = 15880$ g/mol to $\overline{M}_w =$

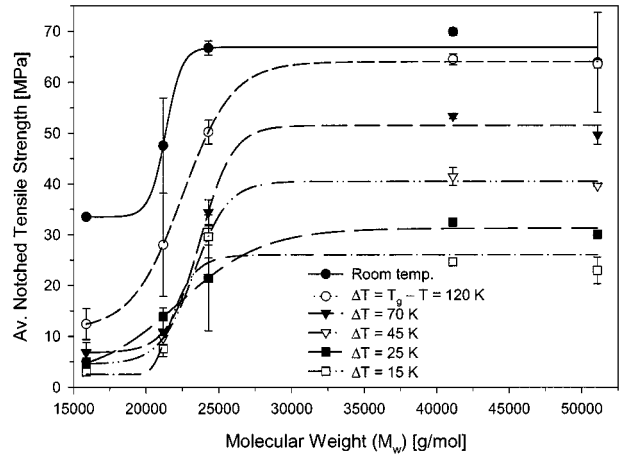

Figure 9 Averaged notched tensile strength plotted as a function of molecular weight at various temperature intervals. Two test specimens were used to calculate the average notched tensile strength.

41100 g/mol, (i.e. across the transition) for successively increasing temperatures, is seen to increase with temperature from approximately 200% at room temperature up to nearly 900% $\Delta T = 45$ K.

3.2. Fractography

The fracture surfaces of each specimen were examined to assess the involvement of different molecular weight-dependent failure mechanisms. Optical photomicrographs of the notched surface after failure are provided in Fig. 10 for all materials and test temperatures – the notch is at the top of each image. This figure illustrates the trends in the fracture events specific to each molecular weight. Examining the image at the juncture of $\overline{M}_w = 41100$ g/mol and $\Delta T = 120$ K, it can be seen that upon moving towards increasing temperature and/or increasing molecular weight (right and/or up), the fracture surfaces are smooth, glasslike and striated in appearance. In moving from this image to the opposite directions, that is to say, lower temperature (left), the fracture surfaces are rough and contain small irregular features. However, moving to lower molecular weight (down), the fracture surfaces become smoother towards higher temperature. Looking at the room temperature column of varying M_w the high M_w fracture surface is rough because of the many nucleation sites of secondary fracture. Moving down the column to successively lower M_w, the introduction of increasingly larger smooth and glasslike regions becomes evident. Thus, the areal surface roughness decreases with M_w. Griffith proposed that a crack propagates when the elastic energy released, is just sufficient to provide the surface energy necessary for the creation of the new surfaces [14]. Therefore, the fracture surfaces of the high M_w materials have a greater areal roughness and consequently have high strain energy release rates [15].

To examine the fracture surfaces in more detail, Fig. 11 contains four enlarged images of the extremes in molecular weight and temperature, taken from Fig. 10. The image at top left (high M_w, low T) shows evidence

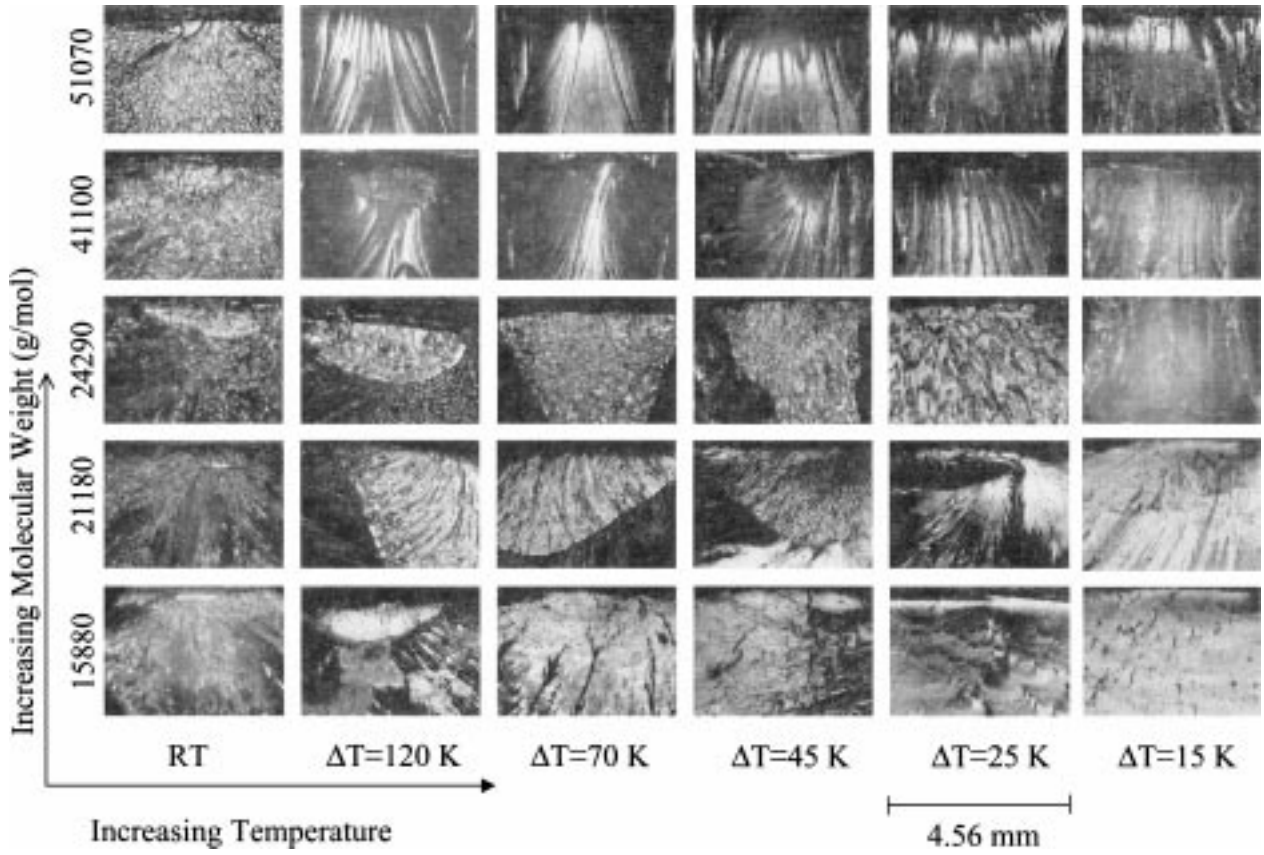

Figure 10 Optical microstructural images taken of the notched fracture surface under a magnification of 25×. The notch is at the top of each image. Images are designated by their weight-average molecular weight and temperature interval below T_g. Each image corresponds to a point on each curve of Fig. 8, for cross-referencing with notched tensile strength properties.

of many parabolic markings (or 'dimple rupture' in metals parlance). A parabolic mark is formed from the interference of two fracture fronts that spread concentrically, from origins that are not in close proximity to each other, such that the primary fracture front can be considered a straight line. The image at the top right (high M_w, high T) illustrates a relatively smooth, glasslike surface with striations, hackles and arrest lines. The lower left image (low M_w, low T) shows a rough surface with no parabolic markings, but the presence of three-dimensional surface-substructures with smooth regions interspersed. This indicates the likelihood of fast crack propagation and is similar to those fracture surfaces observed in epoxy resins with single edge notch geometry and a blunt pre-crack [16]. The lower right image (low M_w, high T) is relatively smooth, but not glasslike, and contains many tear-sites or voids. In addition, the crack front is seen to have propagated in a concentric circular fashion, which is indicative of a stable or constant velocity crack front. Hence, it is clear, from this figure, that there are distinct differences in the failure surfaces for different molecular weight materials as a function of temperature.

3.2. Brittle-ductile behavior

Upon calculation of the yield stress, the brittle to ductile behavior of the materials can be elucidated when the averaged notched tensile strength (y) is plotted as a function of yield stress (x). The line at $y = x$ defines the separation envelope between brittle and ductile behavior, since $y < x$ would be expected to lead to brittle failure and $y > x$ to ductile failure. Fig. 12 is such a plot and it displays the results of all molecular weight variations tested at each of the temperature intervals below T_g. It is clear to see the high molecular weight material has a tendency toward ductile failure and the low molecular weight materials tend towards brittle failure; both independent of temperature. This result is in accord with the temperature-independent, critical molecular weight transition illustrated in Fig. 9, in addition to the stress-strain curves given in Fig. 2a and the differences in elongation to break contained in Fig. 4a and b.

4. Discussion

Over 50 years ago, Flory derived a linear relationship between the stress at brittle failure (σ_b) and the reciprocal number average molecular weight ($\overline{M}_n$) of a polymer [17] to establish a structure-property relationship. Since that time, however, many authors [18–20] have debated the suitability of the $\overline{M}_n$ parameter alone, as a measure for describing mechanical properties. Gent and Thomas suggested that at a critical value of molecular weight, M_c, the onset of a pronounced increase in tensile strength with increase in molecular weight is observed in flexible, non-aromatic polymers [21]. They also popularized the notion that molecules of just sufficient length to form an entangled network in the melt, have a molecular weight, M_e, which is approximately half M_c [21]. Above this

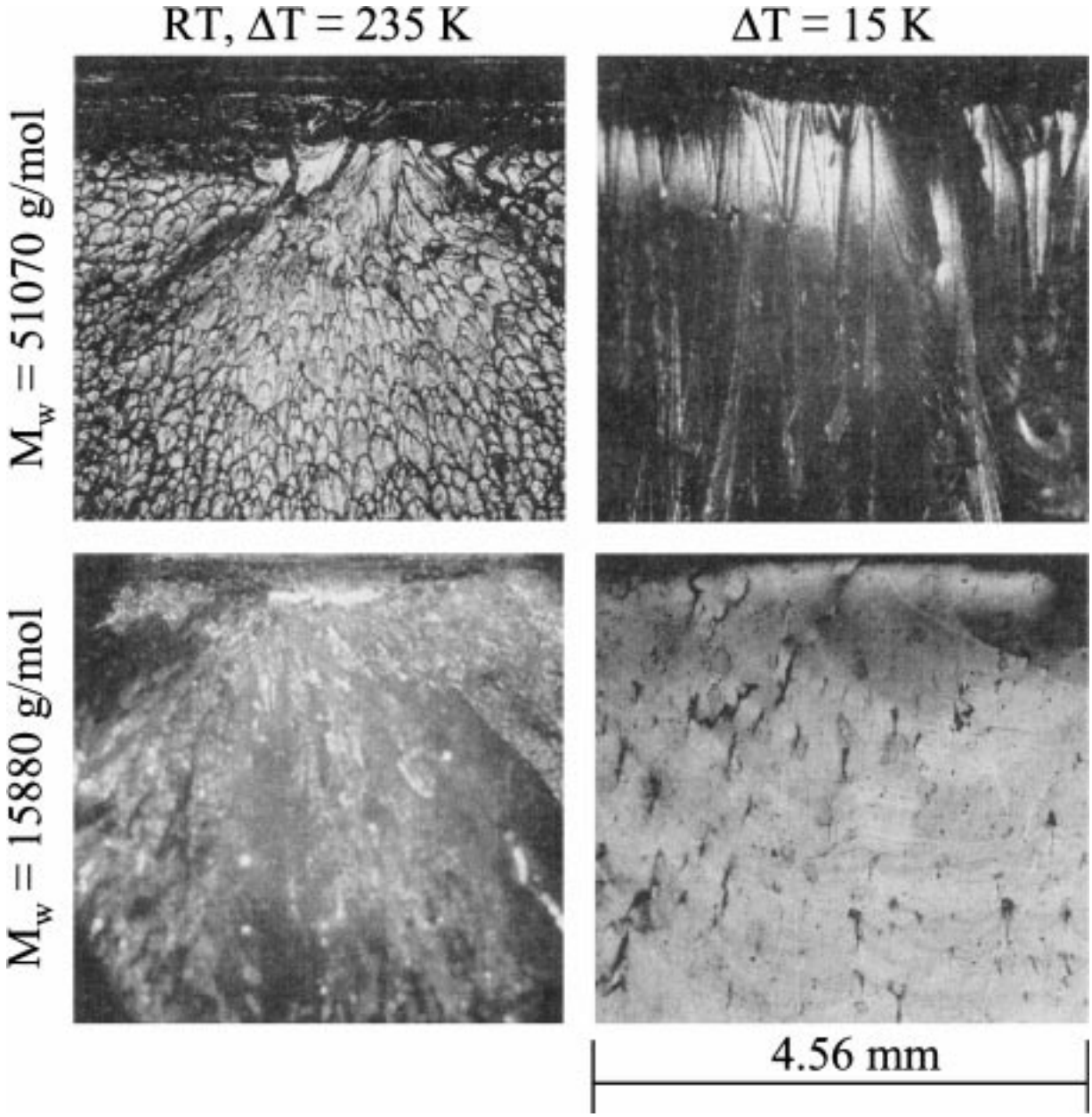

Figure 11 Four microstructural images representative of the extreme conditions in molecular weight and temperature used in this study, enlarged from Fig. 10. Each image is of the notched fracture surface under a magnification of 25×. The notch is at the top of each image.

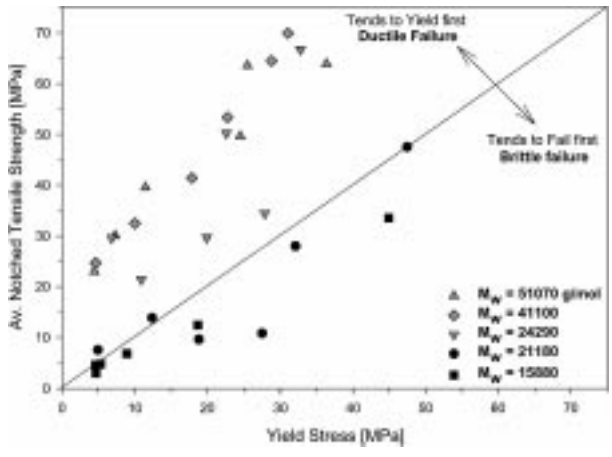

Figure 12 Averaged notched tensile strength plotted as a function of yield stress indicating tendencies towards brittle or ductile failure modes in the LaRC^{TM}-SI materials.

minimum molecular weight needed to form an entangled network, the strength and elongation is known to increase toward a limiting value at high molecular weight [22]. Results indicated in Fig. 9 are in agreement with the premise of a critical molecular weight transition and a limiting value at high molecular weight. It seems apparent then, that the interconnectiveness of molecules via entanglements must account for the increased strength of high molecular weight LaRC^{TM}-SI. At higher molecular weights there may be as many as five entanglements per chain length, calculated for a similar aromatic polyimide [23]. The physical 'knotting' gives added dimensional stability at the microstructural level, thus impeding deformation. This is in agreement with work on strength and fracture toughness of other glassy polymers [24–28].

It is known that plastic deformation of amorphous polymers occurs by crazing or shear-yielding processes

which facilitates the growth of a crack tip [29–31]. Donald and Kramer suggested that, in the fracture of thermoplastics, there is a transition from a crazing to a shear-yielding mechanism when the distance between physical entanglements decreases below ~20 nm [32]. This implies that high M_w materials, with a greater density of chain-entanglements, will tend to shear-yield and low M_w materials will tend to craze. The results presented in Fig. 12 showed the lower molecular weight materials exhibited brittle failure and the higher molecular weight materials showed ductile failure, independent of temperature. A decrease in the molecular weight will cause an increase in the density of chain ends (per unit volume). This collection of ends, or defects within the solid, tend to act as a weakness or stress concentration where brittle failure can be initiated. Failure may take the form of chain scission in which only one bond per chain needs to fail to relieve the stress on the remaining chain segments, or alternatively, the chains may 'pull out' from the new surface as it is formed, rather than undergo scission. Recent work has suggested that chain pull-out dominates at low molecular weights and chain scission prevails at high molecular weights with equal contributions from both mechanisms to the fracture energy at 'mid-range' molecular weights [33, 34]. We have shown, in Fig. 11, that materials with high yield stress have low crack-tip plasticity, stable and continuous crack-growth giving smooth, glasslike surfaces with striations and hackles. Bascom *et al.* have also interpreted these types of surface features as characteristic evidence of a shear-yielding failure mechanism in composite materials [35].

Examination of the fracture surfaces provides an indication of the fracture event but limited information about the deformation and failure process as a whole. Most of the strain energy released in brittle failure is used to create new crack surfaces and to increase the crack propagation speed. Alternatively, the strain energy released in a ductile failure is needed for the plastic deformation (chain extension) and, in comparison, the amount required for the creation of new surfaces is negligible. Thus, at high temperatures, one would expect specimens to yield and show considerable necking compared to those specimens tested at lower temperatures. Indeed, the fracture surfaces of specimens, with $M_w > M_c$ and tested at high temperature, had high deformation indicative of a ductile failure process, yet the smooth fracture surface would indicate a brittle fracture event.

5. Conclusions

The molecular weights, molecular weight distributions, glass transition temperatures and the mechanical response of an advanced thermoplastic, glassy polyimide have been determined. The notched tensile strength is a strong function of both temperature and molecular weight. A critical molecular weight (M_c) is observed to occur at a $\bar{M}_w \sim 22000$ g/mol below which, the notched tensile strength decreases rapidly. This critical molecular weight transition is not temperature dependent. The observed microstructures and non-linear (inelastic) behavior have helped to characterize further, the brittle to ductile transition as a function of molecular weight and temperature. Independent of temperature, high molecular weight materials ($\bar{M}_w > M_c$) will tend to fail in a ductile manner and low molecular weight materials ($\bar{M}_w < M_c$) will tend to exhibit brittle failure. The Young's Modulus and Shear Modulus are strong functions of temperature only.

Acknowledgements

The authors are grateful for: discussions with Dr. S. W. Smith on the fractography; the provision of materials from Imitec, Inc. (Schenectady, NY, USA); the gel permeation chromatography performed by Dr. E. J. Siochi; and the technical assistance of Mr. C. E. Townsley and Mr. R. T. Razon. This work was performed while Dr Nicholson held a National Research Council Research Associateship at NASA Langley Research Center.

References

1. D. WILSON, H. D. STENZENBERGER and P. M. HERGENROTHER, "Polyimides" (Chapman and Hall, New York, 1990).
2. A. K. NOOR, S. M. SPEARING, W. W. ADAMS and S. L. VENNERI, *Aerospace America* April (1998) 24.
3. P. I. VINCENT, *Polymer* **1**(4) (1960) 425.
4. S. MATSUOKA, "Relaxation Phenomena in Polymers" (Hanser, Munich, 1992).
5. M. L. WALLACH, *J. Polym. Sci. A-2* **6** (1968) 953.
6. M. KOCHI, S. ISODA, R. YOKOTA, I. MITA and H. KAMBE, in "Polyimides: Synthesis, Characterization and Applications," edited by K. L. Mittal (Plenum Press, New York, 1984) p. 671ff.
7. W. VOLKSEN, P. COTTS and D. Y. YOON, *J. Polym. Sci. Polym. Phys.* **25** (1987) 2487.
8. E. J. SIOCHI, P. R. YOUNG and R. G. BRYANT, "Materials Challenge - Diversification and the Future, Vol. 40, Part 1," (SAMPE, Los Angeles, California, 1995) p. 11.
9. R. G. BRYANT, *High Perform. Polym.* **8**(4) (1996) 607.
10. T. H. HOU and R. G. BRYANT, *ibid.* **9**(4) (1997) 437.
11. S. S. STERNSTEIN, L. ONGCHIN and A. SILVERMAN, *Appl. Polym. Symp.* **7** (1968) 175.
12. S. S. STERNSTEIN and F. A. MYERS, *J. Macromol. Sci. Phys.* **8** (1973) 539.
13. P. B. BOWDEN, in "The Physics of Glassy Polymers," edited by R. N. Haward (Halsted Press, John Wiley & Sons, New York, 1973) p. 279.
14. A. A. GRIFFITH, *Phil. Trans. Roy. Soc.* **A221** (1921) 163.
15. W. DÖLL, *J. Mater. Sci.* **10** (1975) 935.
16. W. J. CANTWELL and A. C. ROULIN-MOLONEY, in "Fractography and Failure Mechanisms of Polymers and Composites," edited by A. C. Roulin-Moloney (Elsevier Science Publishers Ltd, London, 1989) p. 233.
17. P. J. FLORY, *J. Am. Chem. Soc.* **67** (1945) 2048.
18. R. F. BOYER, *J. Polym. Sci.* **9** (1952) 289.
19. J. M. GOPPEL, in "Plastics Progress," edited by P. Morgan (Iliffe, London, 1960) p. 1.
20. H. W. MCCORMICK, F. M. BROWER and L. KIN, *J. Polym. Sci.* **39** (1959) 87.
21. A. N. GENT and A. G. THOMAS, *ibid. A-2* **10**(3) (1972) 571.
22. E. H. MERZ, L. E. NIELSEN and R. BUCHDAHL, *Ind. Eng. Chem.* **43** (1951) 1396.
23. J. A. HINKLEY and B. J. JENSEN, *High Perform. Polym.* **8** (1996) 599.
24. P. I. VINCENT, *Polymer* **13** (1972) 558.
25. R. P. KUSY, *J. Mater. Sci.* **11** (1976) 1381.
26. R. P. KUSY and D. T. TURNER, *Polymer* **18**(4) (1977) 391.
27. D. T. TURNER, *ibid.* **23** (1982) 626.
28. P. PRENTICE, *ibid.* **24** (1983) 344.

29. R. P. KAMBOUR, *J. Polym. Sci. A* **2** (1964) 4159.
30. *Idem., ibid.* **3** (1965) 1713.
31. S. WELLINGHOF and E. BAER, *J. Macromol. Sci. Phys. B* **11**(3) (1975) 367.
32. A. M. DONALD and E. J. KRAMER, *J. Mater. Sci.* **17** (1982) 1871.
33. P. PRENTICE, *ibid.* **20**(4) (1985) 1445.
34. M. SAMBASIVAM, A. KLEIN and L. H. SPERLING, *J. Appl. Polym. Sci.* **58**(2) (1995) 357.
35. W. D. BASCOM, D. J. BOLL, D. J. FULLER and D. J. PHILLIPS, *J. Mater. Sci.* **20** (1985) 3184.

Received 22 September 1999
and accepted 7 June 2000